

Coupled charm and charmonium transport in a strongly coupled quark-gluon plasma

Kaiyu Fu^{1*}, Biaogang Wu^{1,2} and Ralf Rapp¹

¹*Cyclotron Institute and Department of Physics and Astronomy, Texas A&M University, College Station, TX, 77843-3366, USA.

²Department of Physics, Kent State University, Kent, OH, 44242, USA.

*Corresponding author(s). E-mail(s): kaiyufu@tamu.edu;
Contributing authors: bwu8@kent.edu; rapp@comp.tamu.edu;

Abstract

The quark–gluon plasma (QGP) is a strongly coupled medium in which both open and hidden charm particles experience substantial nonperturbative interactions. This poses a major challenge for a quantitative description of charmonium transport in ultra-relativistic heavy-ion collisions, as it requires a mutually consistent treatment of pertinent transport coefficients. In this work, we present a coupled charm-charmonium transport framework for a strongly coupled QGP based on thermodynamic T -matrix interactions with recent constraints from Wilson-line correlators (WLCs) computed in lattice QCD. For the first time, the same underlying heavy-light interactions and in-medium spectral functions are used to self-consistently evaluate charm-quark diffusion and charmonium kinetics. In particular, the charmonium equilibrium limit, a critical transport parameter for regeneration, is evaluated in the presence of broad spectral functions. Charm-quark diffusion is simulated via Langevin dynamics and coupled to a Boltzmann equation for charmonium dissociation and regeneration. The equilibrium limit of the statistical model is recovered once charm quarks thermalize, and its extension to describe off-equilibrium is constructed. Preliminary applications to charmonium observables in Pb–Pb collisions at the LHC capture the measured centrality and momentum dependence fairly well.

Keywords: strongly coupled quark-gluon plasma, charmonium, T -matrix, coupled transport

| | | | |
|-------------------------------------|----------|---|-----------|
| Contents | | | |
| 1 Introduction | 1 | 4 Charmonia at the LHC | 10 |
| 2 Charm-quark transport | 3 | 4.1 Initial conditions | 10 |
| 2.1 Langevin simulation | 3 | 4.2 Time evolution of Ψ yields | 12 |
| 2.2 Relaxation rate | 4 | 4.3 Centrality dependence | 13 |
| 3 Charmonium transport | 4 | 4.4 Transverse-momentum spectra | 15 |
| 3.1 Boltzmann equation | 5 | 5 Conclusions | 16 |
| 3.2 Nonperturbative rates | 5 | 1 Introduction | |
| 3.3 Equilibrium limit | 8 | The production of charmonium in ultra-relativistic heavy-ion collisions (URHICs) has long | |

been recognized as a suitable probe of the medium modifications of the fundamental Quantum Chromodynamics (QCD) force in the quark–gluon plasma (QGP). Since the original idea that color screening in a deconfined medium would suppress the formation of charmonium bound states [1], extensive theoretical and experimental investigations have revealed that the observed yields result from an interplay of suppression and regeneration mechanisms in the fireball of URHICs [2–5]. In particular, abundant production of $c\bar{c}$ pairs in central collisions of Pb nuclei at the Large Hadron Collider (LHC) led to the prediction of substantial charmonium regeneration [6–8], which was confirmed by experiment.

Quantitative descriptions of charmonium production have been developed using dynamical transport approaches that evaluate the time evolution of the bound states in the expanding fireball. The inelastic reaction rates driving dissociation and regeneration are central to this evolution, as they encode the medium-modified binding energies and radii, as well as the spectral properties of the charmonia which encode their coupling to the thermal partons of the QGP. Many existing transport models rely on perturbative heavy–light interactions and usually require phenomenological K -factors to reproduce the suppression of excited states, such as $\psi(2S)$, in URHICs [9, 10]. These descriptions do not fully capture the dynamics of the strongly coupled QGP (sQGP) [11, 12], as evidenced by the small heavy-quark (HQ) diffusion coefficients extracted from phenomenology [13] and lattice QCD [14], as well as by lattice-QCD based determinations of the HQ potential that exhibit pronounced nonperturbative features [15].

More recent developments in quarkonium transport have moved beyond the perturbative regime through the use of the thermodynamic T -matrix approach [16]. This framework incorporates nonperturbative heavy–light scattering, self-consistent in-medium parton spectral functions (which are strongly broadened), and medium-modified heavy-quark potentials constrained by lattice-QCD calculations of Wilson-line correlators (WLCs) [17]. When deploying pertinent transport coefficients for heavy-quark diffusion to open heavy-flavor phenomenology at the LHC, a decent explanation of heavy-flavor (HF) hadron data can be attained [18]. Quarkonium reaction rates have been computed from the same

underlying interaction as that governing open heavy-flavor transport [19], thus encapsulating the strongly coupled nature of the QGP. Embedding these rates into quarkonium transport models thus establishes a direct connection between quarkonium observables and the microscopic interaction strength of the sQGP, which has been carried out for bottomonia in Pb–Pb and p–Pb collisions at the LHC in Refs. [16, 20].

Strong interactions among the partons in the QGP give rise to broad in-medium spectral functions. The widths of these spectral functions can enhance quarkonium dissociation rates by enabling off-shell scattering which increases the available phase-space for the outgoing light partons and charm quarks. However, a recent T -matrix study in the complex-energy plane revealed that large in-medium widths do not necessarily imply the disappearance of quarkonium states [21]. Instead, quarkonium poles can persist to high temperatures while acquiring large widths, indicating robust $Q\bar{Q}$ correlations in the form of resonances over a broad temperature range. This extends the effective regeneration window during the fireball evolution and, in combination with large reaction rates, drives quarkonia toward their equilibrium limits rather rapidly. A proper treatment of the charmonium equilibrium limit in the presence of broad spectral functions is therefore essential for reliably determining the final charmonium yields.

Another essential ingredient for the charmonium equilibrium limit is the kinetic evolution of charm quarks. Charm and anticharm quarks produced in initial hard scatterings are far from thermal equilibrium but gradually approach it through diffusion and drag in the medium. Their time-dependent momentum distributions directly impact the magnitude and momentum dependence of regenerated charmonia [22, 23]. Langevin simulations provide an effective framework for describing HQ diffusion in the QGP [24–26] and enable one to track the time evolution of charm quarks throughout the evolution of the fireball [27]. The key inputs to these simulations are the HQ transport coefficients, that are, in principle, closely related to the quarkonium reaction rates.

In the present paper we build on earlier work [27] but with several key improvements, that, in particular, are based on much more realistic

interactions rooted in the sQGP, along with the required technical developments. While Ref. [27] relied on perturbative reaction rates, we here, for the first time, employ a universal underlying heavy-light interaction together with off-shell spectral functions to compute both charm-quark and charmonium transport coefficients. Time-dependent off-equilibrium charm-quark distributions obtained from Langevin simulations are coupled to charmonium regeneration in the Boltzmann transport equation governing charmonium kinetics. In particular, the equilibrium limit is formulated (and validated) through the ratio of dissociation and regeneration rates, which enables a controlled implementation of the in-medium spectral functions of charm quarks and thermal partons. As a preliminary test, we also compute charmonium observables at the LHC using a schematic fireball expansion for the medium evolution (albeit with an improved equation of state compatible with lattice QCD).

The remainder of this paper is organized as follows. In Sec. 2 we briefly recall the Langevin dynamics used to simulate charm-quark diffusion in the QGP and the calculation of the corresponding transport coefficients from the in-medium T -matrix. In Sec. 3, we introduce the Boltzmann equation for charmonium transport including the derivation of charmonium dissociation and regeneration rates from the same T -matrix interactions. In particular, we obtain the regeneration rates using off-shell spectral functions while satisfying detailed balance and ensuring the correct equilibrium limit, stipulating the connection between off-equilibrium charm-quark and charmonium transport. In Sec. 4, we turn to our applications to observables, specifying the phenomenological inputs from pp spectra, cold-nuclear-matter effects, and the time evolution of the medium and presenting our results for charmonium nuclear modification factors R_{AA} in Pb–Pb collisions at the LHC. Finally, Sec. 5 contains a summary and outlook.

2 Charm-quark transport

In this section, we recall the relativistic Langevin approach to simulate HQ diffusion in the QGP (Sec. 2.1) and discuss the calculation of the charm-quark transport coefficient, *i.e.*, the relaxation

rate, from the nonperturbative T -matrix approach (Sec. 2.2).

2.1 Langevin simulation

Heavy quarks, *i.e.*, charm or bottom, have masses, m_Q , that are much larger than typical medium temperatures in URHICs ($m_Q \gg T$) and momentum transfers in a single scattering, which are small compared to the momentum ($\Delta p \ll m_Q$). Under these conditions, the evolution of the charm-quark phase-space distribution, f_c , can be described by a Fokker–Planck equation [25],

$$\frac{\partial}{\partial t} f_c(t, \mathbf{p}) = \frac{\partial}{\partial p_i} \left[\Gamma(\mathbf{p}) p_i f_c(t, \mathbf{p}) + D(\mathbf{p}) \frac{\partial}{\partial p_i} f_c(t, \mathbf{p}) \right], \quad (1)$$

where \mathbf{p} is the charm-quark three-momentum and $\Gamma(\mathbf{p})$ and $D(\mathbf{p})$ are the friction and momentum diffusion coefficients, respectively.

Relativistic Langevin dynamics in expanding media has been widely employed in phenomenological studies of HF transport [24, 28–30]. It preserves the correct local thermalization behavior dictated by the underlying Fokker–Planck equation, while enabling an efficient simulation of the diffusion process in space-time-dependent backgrounds.

In the post-point scheme [30], the equilibrium conditions (Einstein relations) read

$$\begin{aligned} D(\mathbf{p}) &= \Gamma(\mathbf{p}) E T, \\ \Gamma(\mathbf{p}) &= A(\mathbf{p}) + \frac{1}{E} \frac{\partial D}{\partial E}, \end{aligned} \quad (2)$$

where $A(\mathbf{p})$ is the drag coefficient representing the thermal relaxation rate (T : medium temperature). The momentum diffusion coefficient $D(\mathbf{p})$ is obtained from $A(\mathbf{p})$ via the Einstein relation.

The Fokker–Planck equation can be realized numerically through a set of stochastic Langevin equations [30],

$$\begin{aligned} dx_i &= \frac{p_i}{E} dt, \\ dp_i &= -\Gamma(\mathbf{p}) p_i dt + \sqrt{2 D(|\mathbf{p} + d\mathbf{p}|)} dt \rho_i, \end{aligned} \quad (3)$$

where $E = \sqrt{\mathbf{p}^2 + m_c^2}$ denotes the charm quark's energy and x_i and p_i ($i = 1, 2, 3$) are its spatial and momentum components, respectively. The stochastic variables ρ_i are Gaussian-distributed random numbers satisfying $\langle \rho_i \rangle = 0$ and $\langle \rho_i \rho_j \rangle = \delta_{ij}$, with a probability distribution $P(\rho) = (2\pi)^{-3/2} \exp(-\rho^2/2)$. The coordinate update is straightforward using the velocity determined by the current momentum. The momentum update is carried out in the local rest frame of the medium, in which the drag and diffusion coefficients are defined. First, a provisional momentum increment is computed using the drag and diffusion coefficients evaluated at the initial momentum \mathbf{p} . Subsequently, the diffusion term is evaluated at the updated momentum magnitude $|\mathbf{p} + d\mathbf{p}|$,

$$dp_i^{\text{diff}} = \sqrt{2D(|\mathbf{p} + d\mathbf{p}|)} dt \rho_i, \quad (4)$$

and combined with the drag contribution, $dp_i^{\text{drag}} = -\Gamma(\mathbf{p}) p_i dt$, to obtain the total momentum increment dp_i . The same time step dt and stochastic noise ρ_i are used in both steps. After each time step, the updated momentum is Lorentz-boosted back to the laboratory frame.

2.2 Relaxation rate

The key input to the HQ Langevin simulation is the relaxation rate which encodes the interaction strength between the heavy quark and the medium constituents. We calculate it using nonperturbative T -matrices with recent constraints from WLCs computed in lattice QCD [15]. Of particular importance are off-shell effects which enable the c -quark to access interaction strength that is encoded in D -meson bound states that are located below the nominal charm light-quark threshold. The pertinent expression has been derived from the Kadanoff-Baym equations in Ref. [31]. For an incoming (on-shell) c -quark of momentum \mathbf{p}_c one obtains

$$A(\mathbf{p}_c) = \sum_i \int d\mathbf{\Pi} \frac{1}{d_c} |\mathcal{M}_{ic \rightarrow ic}|^2 \times \rho_c(\omega', \mathbf{p}'_c) \rho_i(\nu, \mathbf{q}) \rho_i(\nu', \mathbf{q}') \times [1 - n_c(\omega')] n_i(\nu) [1 \pm n_i(\nu')] \left(1 - \frac{\mathbf{p}_c \cdot \mathbf{p}'_c}{\mathbf{p}_c^2}\right), \quad (5)$$

where the off-shell effects are encoded in the heavy-light scattering amplitude, $\mathcal{M}_{ic \rightarrow ic}$, and in

the spectral functions, $\rho_{i,c}$, of the light thermal partons ($i = u, \bar{u}, d, \bar{d}, s, \bar{s}, g$ with 4-momenta (ν, \mathbf{q}) and (ν', \mathbf{q}') for the incoming and outgoing ones, respectively) and the outgoing c -quark of momentum \mathbf{p}'_c . The corresponding on-shell energies, $\varepsilon_i(\mathbf{q}) = \sqrt{m_i^2 + \mathbf{q}^2}$ and $\varepsilon_c(\mathbf{p}_c) = \sqrt{m_c^2 + \mathbf{p}_c^2}$, figure in the integration measure,

$$d\mathbf{\Pi} = \frac{d\omega' d^3\mathbf{p}'_c}{(2\pi)^3 2\varepsilon_c(\mathbf{p}'_c)} \frac{d\nu d^3\mathbf{q}}{(2\pi)^3 2\varepsilon_i(\mathbf{q})} \frac{d\nu' d^3\mathbf{q}'}{(2\pi)^3 2\varepsilon_i(\mathbf{q}')} \times (2\pi)^4 \delta^{(3)}(\mathbf{p}_c + \mathbf{q} - \mathbf{p}'_c - \mathbf{q}') \times \frac{1}{2\varepsilon_c(\mathbf{p}_c)} \delta(\varepsilon_c(\mathbf{p}_c) + \nu - \omega' - \nu'), \quad (6)$$

which also contains the energy-momentum conserving δ -functions. The c -quark's color-spin degeneracy is $d_c=6$, and n is the Fermi-Dirac (Bose-Einstein) distribution for fermions (bosons).

The heavy-light scattering amplitude, $|\mathcal{M}_{ic \rightarrow ic}|^2$, is directly related to the T -matrix which we evaluate in the center-of-mass frame, including the sum over all relevant color and partial-wave channels [31]. For later use we introduce the spin-color averaged matrix element,

$$\overline{|\mathcal{M}_{ic \rightarrow ic}|^2} = \frac{|\mathcal{M}_{ic \rightarrow ic}|^2}{d_i d_c}, \quad (7)$$

where d_i denotes the color-spin degeneracy of the light partons, $d_{q/\bar{q}} = 6$ and $d_g = 16$.

In Fig. 1 we show the charm-quark relaxation rate as a function of 3-momentum, $p = |\mathbf{p}_c|$, at different temperatures. Its momentum dependence features a marked enhancement at low momenta where nonperturbative effects are most significant which was previously mimicked by perturbative reaction rates with a large K factor [27].

3 Charmonium transport

In this section, we outline the transport framework for charmonia in the QGP. In Sec. 3.1, we introduce the Boltzmann transport equation and its formal solution, which separates into primordial and regeneration components. In Sec. 3.2, we construct the nonperturbative dissociation and regeneration rates and elucidate their connection to charm-quark transport, thereby verifying the proper detailed balance relation in the limit of

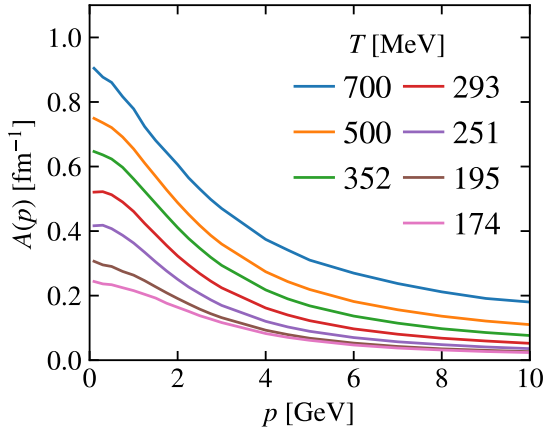


Fig. 1: The charm-quark relaxation rate, $A(p)$, as a function of momentum at different temperatures from T -matrices constrained by WLCs from lattice QCD [15].

thermalized charm quarks. This requires a discussion of the charmonium equilibrium limit in the presence of off-shell effects, which is given in Sec. 3.3.

3.1 Boltzmann equation

The transition between bound charmonium states, $\Psi = J/\psi, \chi_c, \psi(2S)$, and uncorrelated charm-anticharm pairs in the medium can be evaluated in semiclassical approximation using the Boltzmann transport equation,

$$\frac{\partial f_\Psi}{\partial t} + \mathbf{v} \cdot \nabla f_\Psi = -\alpha(\mathbf{P}_\Psi, T) f_\Psi + \beta(\mathbf{P}_\Psi, T), \quad (8)$$

where

$$f_\Psi(\mathbf{x}, \mathbf{P}_\Psi, t) \equiv \frac{dN_\Psi}{d^3x d^3P_\Psi}, \quad (9)$$

is the phase-space distribution function of a charmonium state of momentum \mathbf{P}_Ψ at position \mathbf{x} , and its velocity $\mathbf{v} = \mathbf{P}_\Psi/E_\Psi$ with energy $E_\Psi = \sqrt{\mathbf{P}_\Psi^2 + M_\Psi^2}$.

The formal solution of Eq. (8) amounts to a sum of a primordial-survival contribution and a continuous regeneration contribution [32],

$$f(\mathbf{x}, \mathbf{P}_\Psi, t) = f(\mathbf{x}(t, t_0), \mathbf{P}_\Psi, t_0) e^{-\int_{t_0}^t dt' \alpha(\mathbf{P}_\Psi, T(t'))} + \int_{t_0}^t dt' \beta(\mathbf{P}_\Psi, T(t')) e^{-\int_{t'}^t dt'' \alpha(\mathbf{P}_\Psi, T(t''))}, \quad (10)$$

where $\mathbf{x}(t, t') \equiv \mathbf{x} - \mathbf{v}(t - t')$ represents the classical charmonium trajectory. The first term in Eq. (10) tracks the primordial charmonium component produced from initial hard scatterings. When propagating through the evolving medium, it undergoes a gradual dissociation governed by the in-medium rate α (we neglect elastic rescattering which is suppressed by the bound-state phase space). The second term accounts for charmonium regeneration from charm-anticharm pairs, which commences at the dissociation temperature and continues until freezeout. The incremental gain, βdt , is produced locally in the medium and thus inherits the collective flow of the surrounding fluid (imparted to the charm quarks), and subsequently it is subject to the same dissociation processes as the primordial component. The time integral therefore reflects the competition between continuous regeneration and subsequent in-medium suppression, driving the total yields towards their equilibrium.

3.2 Nonperturbative rates

In Fig. 2 we pictorially illustrate the dissociation and regeneration mechanisms of charmonia in the QGP. We employ a quasifree approximation [19, 33], where the $2 \rightarrow 3$ dissociation process (upper panel) is reduced to an inelastic (half off-shell) $2 \rightarrow 2$ scattering process of a thermal-medium parton off the charm (anticharm) quark, while the anticharm (charm) quark acts as a spectator and the charmonium binding energy is incorporated into an effective charm-quark mass,

$$\tilde{m}_c = m_c - E_B^\Psi. \quad (11)$$

The in-medium charm-quark mass, m_c , and charmonium binding energies, E_B^Ψ , are determined from the same in-medium T -matrix formalism as the heavy-light amplitudes [15]. For a charmonium 3-momentum \mathbf{P}_Ψ the momenta of the charm and anticharm quarks are assigned proportionally to their effective masses,

$$\mathbf{p}_c = \frac{\tilde{m}_c}{M_\Psi} \mathbf{P}_\Psi, \quad \mathbf{p}_{\bar{c}} = \frac{m_c}{M_\Psi} \mathbf{P}_\Psi, \quad (12)$$

which ensures equal velocities and preserves relativistic energy-momentum conservation. The charmonium energy is simply the sum of the energies

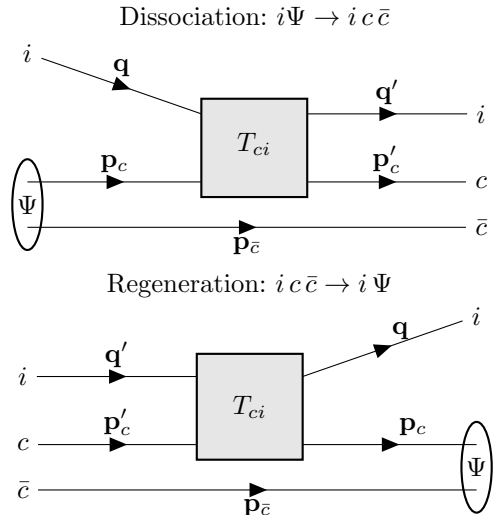


Fig. 2: Schematic T -matrix diagrams illustrating the dissociation and regeneration of charmonium in the QGP. *Upper panel:* dissociation process $i\Psi \rightarrow ic\bar{c}$, in which a thermal parton i scatters off a bound charmonium state Ψ , leading to its breakup into an unbound charm–anticharm pair. *Lower panel:* inverse process of regeneration $ic\bar{c} \rightarrow i\Psi$, where an uncorrelated $c\bar{c}$ pair recombines into charmonium through an interaction with a thermal parton. In both cases, the interaction is described by the half-off-shell T -matrix amplitude T_{ci} . The 3-momenta of the thermal partons and heavy quarks are indicated explicitly.

of the quasifree charm quark and the spectator anticharm quark,

$$E_{\Psi}(\mathbf{P}_{\Psi}) = \varepsilon_c(\mathbf{p}_c) + \varepsilon_{\bar{c}}(\mathbf{p}_{\bar{c}}). \quad (13)$$

Energy conservation in the $2 \rightarrow 3$ ($3 \rightarrow 2$) process reads

$$E_{\Psi}(\mathbf{P}_{\Psi}) + \nu = \omega' + \nu' + \varepsilon_{\bar{c}}(\mathbf{p}_{\bar{c}}), \quad (14)$$

and reduces to

$$\varepsilon_c(\mathbf{p}_c) + \nu = \omega' + \nu', \quad (15)$$

for the $2 \rightarrow 2$ process. This equivalence is critical for recovering the correct equilibrium limit, as will be elaborated in the derivation of the regeneration rate in Sec. 3.3.

The final expression for the charmonium dissociation rate is given by [19, 31]

$$\begin{aligned} \alpha(\mathbf{P}_{\Psi}, T(t)) = & 2 \sum_i d_i \int d\Pi |\overline{\mathcal{M}}_{ic \rightarrow ic}|^2 \\ & \times \rho_c(\omega', \mathbf{p}'_c) \rho_i(\nu, \mathbf{q}) \rho_i(\nu', \mathbf{q}') \\ & \times (1 - n_c(\omega')) n_i(\nu) (1 \pm n_i(\nu')) (1 - n_{\bar{c}}(\varepsilon_{\bar{c}})) \\ & \times [1 - e^{i\mathbf{k} \cdot \mathbf{r}}], \end{aligned} \quad (16)$$

where the sum runs over thermal partons $i = q, \bar{q}, g$. The phase-space integration measure $d\Pi$ is defined in Eq. (6), but with a "quasifree" (off-shell) incoming charm quark. The scattering matrix and spectral functions are identical to those in Eq. (5), but with the addition of a Pauli-blocking factor for the spectator anticharm quark (which is numerically immaterial). The factor $1 - e^{i\mathbf{k} \cdot \mathbf{r}}$ accounts for the interference between charm–light and anticharm–light scattering amplitudes [34], where $\mathbf{k} = \mathbf{p}'_c - \mathbf{p}_c$ denotes the momentum transfer and \mathbf{r} characterizes the spatial size of the charmonium bound state (see Fig. 15 in Ref. [19]). For large charmonium radii, the rapidly oscillating phase suppresses the interference term, effectively turning off interference effects, while destructive interference causes the rate to vanish in the limit $r \rightarrow 0$.

In Fig. 3 we collect the resulting rates as a function of 3-momentum and for different temperatures for the three charmonium states considered in this work. A clear hierarchy is observed in terms of the binding energy of the different states with smaller values leading to larger dissociation widths (rates). Compared to the perturbative dissociation rates employed in our previous works [10], the nonperturbative rates are substantially larger, especially for the excited states. Moreover, the momentum dependence of the nonperturbative rates differs qualitatively from that of the perturbative calculations: while the nonperturbative rates decrease with increasing momentum, the leading-order perturbative rates exhibit an increasing trend with momentum. We also make use of a T -matrix pole analysis of the in-medium charmonium spectrum in the complex energy plane [21], which indicates that the J/ψ , χ_c , and $\psi(2S)$ states persist up to temperatures of about 500, 350 and 250 MeV, respectively. These temperatures, which are generally higher than

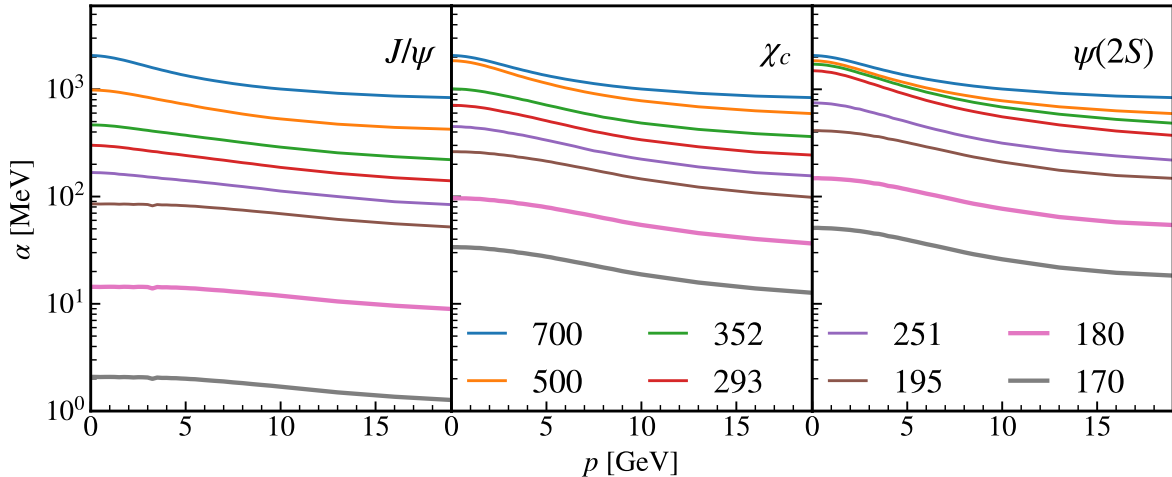


Fig. 3: Dissociation rates of three charmonium states calculated within the nonperturbative T -matrix formalism in the WLC scenarios, shown as functions of their momenta at different temperatures (different colors). From left to right, the panels correspond to J/ψ , χ_c , and $\psi(2S)$.

where the binding energies vanish, are used to determine the onset of the regeneration processes in the transport simulations.

For temperatures below 195 MeV, the rates are obtained by interpolation between the 195 MeV results and the hadronic rates at 170 MeV at $p = 0$ GeV [9], while preserving the momentum dependence of the 195 MeV results. In Fig. 4 we summarize the temperature dependence of the rates at vanishing charmonium momentum. They nicely exhibit the expected hierarchy based on their vacuum binding properties which not only includes the binding energy but also interference effects due to their different sizes which increasingly suppress the rates at smaller radii (also referred to as the imaginary part of the potential). When the state dissolves, the rates level off at twice the collision rate of the constituent charm quarks; toward lower temperatures the interference effects kick in first followed by another drop induced by the transition into the hadronic phase, while the reduction due to finite binding energies is much more gradual (and strongly smeared out due to the large widths of the charm-quark spectral functions).

We now turn to the regeneration rate, β , which to our knowledge is the first time that it has been worked out with off-shell spectral functions. We start from the detailed-balance relation in thermal

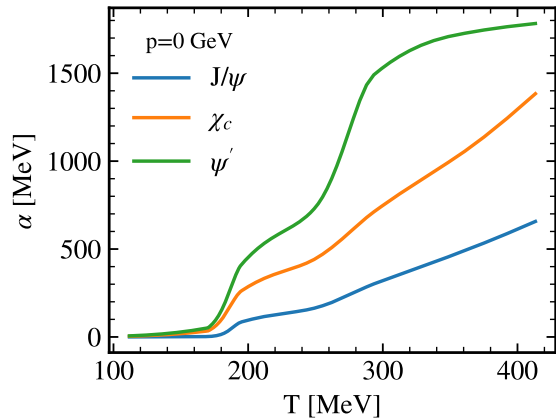


Fig. 4: Charmonium dissociation rates at vanishing three-momentum as a function of temperature.

equilibrium [27],

$$\beta(\mathbf{P}_\Psi, T) = \gamma_c^2 d_\Psi e^{-E_\Psi(\mathbf{P}_\Psi)/T} \alpha(\mathbf{P}_\Psi, T), \quad (17)$$

where γ_c is the charm-quark fugacity that accounts for charm-number conservation in the medium [35, 36], and d_Ψ is the spin degeneracy of each charmonium state (we use 8 for the near-degenerate $\chi_c(1P)$ states). By energy conservation, the Boltzmann factor in Eq. (14) takes the

form

$$e^{-E_\Psi(\mathbf{P}_\Psi)/T} = e^{-(\omega' + \nu' - \nu + \varepsilon_{\bar{c}})/T}. \quad (18)$$

We further employ the identity,

$$n(E) = e^{-E/T} (1 \pm n(E)), \quad (19)$$

(where the upper (lower) sign applies to bosons (fermions)) which allows us to rewrite Boltzmann factors into quantum-statistical distribution functions and their pertinent Bose-enhancement or Pauli-blocking factors. Combining Eqs. (16), (17), (18), and (19), we then obtain the regeneration rate in thermal equilibrium as

$$\begin{aligned} \beta(\mathbf{P}_\Psi, T) &= 2\gamma_c^2 \sum_i d_\Psi d_i \int d\Pi \overline{|\mathcal{M}_{ic \rightarrow ic}|^2} \\ &\times \rho_c(\omega', \mathbf{p}'_c) \rho_i(\nu, \mathbf{q}) \rho_i(\nu', \mathbf{q}') \\ &\times n_c(\omega') [1 \pm n_i(\nu)] n_i(\nu') n_{\bar{c}}(\varepsilon_{\bar{c}}) \\ &\times [1 - e^{i\mathbf{k} \cdot \mathbf{r}}] \end{aligned} \quad (20)$$

where all distribution functions correspond to thermal equilibrium. For dissociation, the incoming c -quark is taken to be on shell, while the incoming and outgoing light partons i and the outgoing c -quark are treated off shell. For regeneration, where the quarkonium appears in the final state, the on-shell and off-shell assignments are interchanged relative to dissociation: the outgoing c -quark is taken as on-shell, whereas the incoming heavy quark and the incoming and outgoing light partons i remain off-shell. The spectator quark is on-shell in both rates.

Off-equilibrium charm quarks can now be implemented into the regeneration processes by replacing the charm-quark distribution functions, n_c , with $f_c(p, t)$ from the Langevin simulations. This is straightforward for the on-shell distribution function, $n_{\bar{c}}(\varepsilon_{\bar{c}})$, where the on-shell energy is directly available from the semiclassical Langevin simulation at each time step. But it requires some care for the off-shell case, $n_c(\omega')$. It turns out that an additional factor $e^{-[\omega' - \varepsilon_c(\mathbf{p}'_c)]/T(t)}$, which essentially represents a thermal off-shell weighting, results in the correct equilibrium limit. The thermal off-equilibrium and off-shell regeneration

rate is thus given by

$$\begin{aligned} \beta(\mathbf{P}_\Psi, T(t)) &= 2\gamma_c^2 \sum_i d_\Psi d_i \int d\Pi \overline{|\mathcal{M}_{ic \rightarrow ic}|^2} \\ &\times \rho_c(\omega', \mathbf{p}'_c) \rho_i(\nu, \mathbf{q}) \rho_i(\nu', \mathbf{q}') \\ &\times [1 \pm n_i(\nu)] n_i(\nu') \\ &\times f_c(\mathbf{p}'_c, T(t)) e^{-[\omega' - \varepsilon_c(\mathbf{p}'_c)]/T(t)} \\ &\times f_{\bar{c}}(\mathbf{p}_{\bar{c}}, T(t)) [1 - e^{i\mathbf{k} \cdot \mathbf{r}}]. \end{aligned} \quad (21)$$

In the limit where charm quarks are fully thermalized, the non-equilibrium distribution becomes

$$f_c(\mathbf{p}'_c, T(t)) \rightarrow e^{-\varepsilon_c(\mathbf{p}'_c)/T(t)}, \quad (22)$$

which renders the Boltzmann factor in Eq. (21)

$$f_c(\mathbf{p}'_c, T(t)) e^{-[\omega' - \varepsilon_c(\mathbf{p}'_c)]/T(t)} \rightarrow e^{-\omega'/T(t)}, \quad (23)$$

thus recovering Eq. (20).

3.3 Equilibrium limit

The equilibrium limit of charmonia plays a key role in their kinetics. Since charm-quark number is conserved, it depends on the interplay with the open-charm spectrum in the medium which is encoded in the fugacity factor (or chemical potential) introduced in Eq. (17). The relative chemical equilibrium in the charm-quark sector thus depends on the charm-quark masses and charmonium binding energies which in turn determine the charmonium masses. This can be directly gleaned from the stationary (long-time) limit of the Boltzmann equation Eq. (8),

$$\frac{df_\Psi}{dt} = 0, \quad (24)$$

which leads to the detailed-balance condition

$$f_\Psi^{\text{eq}}(\mathbf{x}, \mathbf{p}, t) = \frac{\beta(\mathbf{x}, \mathbf{p}, t)}{\alpha(\mathbf{x}, \mathbf{p}, t)}, \quad (25)$$

and thus

$$f_\Psi^{\text{eq}}(\mathbf{x}, \mathbf{p}, t) = \gamma_c^2 d_\Psi e^{-E_\Psi/T(t)}. \quad (26)$$

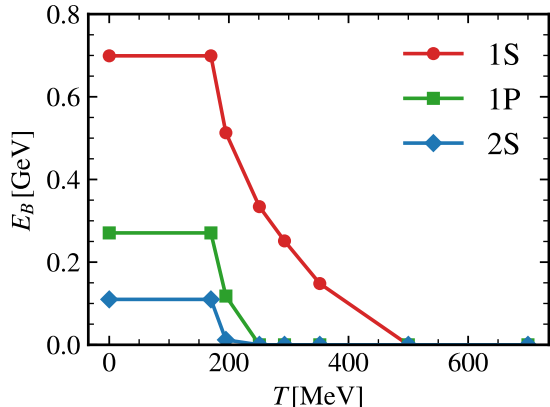


Fig. 5: Binding energies of J/ψ , χ_c and $\psi(2S)$ as a function of temperature, extracted from the in-medium T -matrix approach in the WLC scenario.

The in-medium charm-quark mass and charmonium binding energies are taken from the thermodynamic T -matrix constrained by the lattice-QCD results of the WLCs [19] and are shown in Figs. 5 and 6, respectively.

The charm-quark fugacity, γ_c , is fixed by the total number of produced charm-quark pairs, $N_{c\bar{c}}$, in the fireball of a heavy-ion collision,

$$N_{c\bar{c}} = \frac{1}{2} \gamma_c n_{\text{op}} V_{\text{FB}} \frac{I_1(\gamma_c n_{\text{op}} V_{\text{co}})}{I_0(\gamma_c n_{\text{op}} V_{\text{co}})} + \gamma_c^2 n_{\text{hid}} V_{\text{FB}}, \quad (27)$$

where V_{FB} is the (time-dependent) fireball volume, and n_{op} and n_{hid} denote the densities of open and hidden charm states at a given temperature, respectively (the latter is usually negligible); I_0 and I_1 are the modified Bessel functions; V_{co} denotes the correlation volume that accounts for the local conservation of charm number in the canonical ensemble [33, 35, 37], which is particularly relevant if only one (or a few) pair(s) are present which effectively increases the local $c\bar{c}$ density. We follow our previous treatment which accounts for a time-dependent expansion as $V_{\text{co}}(\tau) = \frac{4\pi}{3} (r_0 + \langle v_c \rangle \tau)^3$ where $r_0 \simeq 1.2$ fm is an initial radius and $\langle v_c \rangle = 0.6$ a typical recoil velocity of the charm quarks. When the system contains multiple charm-quark pairs, their correlation volumes overlap and the system transitions to the grand-canonical ensemble, *i.e.*, the correlation volume is replaced by the fireball volume, $V_{\text{co}} \rightarrow V_{\text{FB}}$. In this work, we use the condition

$N_{c\bar{c}} V_{\text{co}} > \kappa V_{\text{FB}}$ to switch from the canonical to the grand-canonical ensemble. Our default value $\kappa=1$ renders a continuous transition, but we have checked that the regeneration yields in Pb–Pb collisions are hardly affected by varying κ in either semi-/central collisions (where the abundant charm production puts the system into the grand-canonical regime already at early times) or peripheral collisions (where the average $c\bar{c}$ number is well below 1 so that the system remains in the canonical regime throughout the evolution). The main sensitivity arises at intermediate centralities (around $N_{\text{part}} \simeq 100$), where typically 1–2 $c\bar{c}$ pairs are present: *e.g.*, reducing κ from 1 to 0.5 leads to an earlier transition to the grand-canonical ensemble, lowering the equilibrium limit and reducing the regenerated charmonium yield by about 10–20%.

The open-charm density, n_{op} , in the QGP phase was previously estimated by including both the charm quarks and the lowest-lying S -wave D -meson states (D , D^* , D_s , and D_s^*) [35]. In this work, we instead employ only charm quarks but with an effective mass, $m_c^*(T)$, that is constrained by fitting the lattice-QCD results for the (dimensionless) charm-quark number susceptibility [38, 39]:

$$\chi_2^c = \frac{2d_c}{(2\pi T)^3} \int d^3\mathbf{p} e^{-E_p/T}, \quad (28)$$

with $E_p = \sqrt{p^2 + m_c^{*2}(T)}$, $d_c=6$ and an extra factor 2 to account for charm and anticharm quarks. By fitting the lattice-QCD data for the charm-quark number susceptibility, shown in the upper panel of Fig. 6, we extract the temperature dependence of the effective charm-quark mass which is displayed in the lower panel of Fig. 6. At a temperature of $T_{\text{H}} = 170$ MeV, where we convert from partonic to hadronic degrees of freedom in our transport parameters, we have ensured that the effective charm-quark mass provides a smooth matching of the open-charm density of the hadronic phase, specifically the hadron resonance gas model [9]. The resulting effective charm-quark mass is approximately 1.46 GeV at $T = 500$ MeV and increases to about 1.76 GeV at T_{H} . We emphasize that the effective mass is only used in the open-charm density for the sole purpose of obtaining the charm fugacity, to mimic the emergence of pre-hadronic states as the hadronization temperature is approached from above (the transport

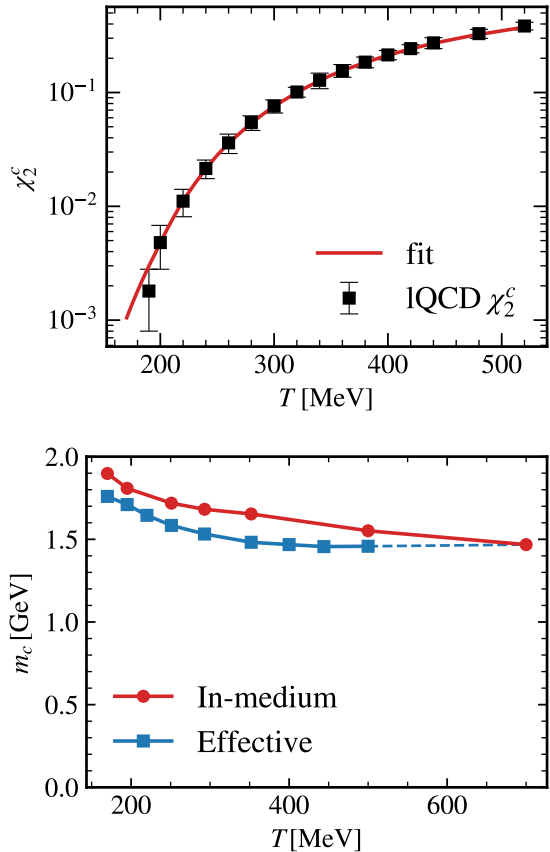


Fig. 6: Upper panel: Charm-quark number susceptibility from lattice-QCD calculations [38] compared to the quasiparticle model with an effective charm-quark mass. Lower panel: In-medium charm-quark mass extracted from the T -matrix in the WLC scenario, together with the effective charm-quark mass, as functions of temperature.

calculations are entirely based on the in-medium masses from the T -matrix analysis [15]). This is also reflected by the fact that the effective mass is noticeably smaller than the in-medium mass, cf. Fig. 6, which results in a larger open-charm density, effectively representing the resonance states contribution. Even at temperatures as high as 500 MeV, the effective mass is still somewhat smaller than the in-medium mass, indicating the presence of resonance-like correlations as found in the complex pole analysis of the T -matrix with WLC constraints [21].

4 Charmonia at the LHC

We now turn to applications of our new transport framework to experiment by coupling it to a schematic fireball model for Pb–Pb collisions at $\sqrt{s_{\text{NN}}} = 5.02$ TeV at the LHC, focusing on the centrality and momentum dependence of charmonium production. In Sec. 4.1, we specify the inputs to our approach, specifically the charm/onium cross sections, including their transverse-momentum (p_{T}) dependence and cold-nuclear-matter modifications. In Sec. 4.2 we discuss the time evolution of the charmonium equilibrium limits under the conditions of the fireball formed in Pb–Pb collisions. In Secs. 4.3 and 4.4 we show our results for the centrality and p_{T} -dependence of J/ψ , χ_c and $\psi(2S)$ production in comparison to experimental data and highlight the main differences to previous calculations.

The main observable is the nuclear modification factor, R_{AA} , defined as the ratio of the charmonium yield in nucleus–nucleus (AA) collisions, N_{ψ}^{AA} , to the one in proton–proton (pp) collisions scaled by the number, N_{coll} , of binary collisions for a given centrality selection,

$$R_{\text{AA}}^{\psi}(N_{\text{part}}, p_{\text{T}}) = \frac{N_{\psi}^{\text{AA}}(N_{\text{part}}, p_{\text{T}})}{N_{\psi}^{\text{PP}}(p_{\text{T}}) N_{\text{coll}}(N_{\text{part}})}, \quad (29)$$

where N_{part} is the number of participant nucleons characterizing the collision centrality.

4.1 Initial conditions

The differential J/ψ production cross section in 5.02 TeV pp collisions has been measured as $d\sigma_{J/\psi}/dy = 5.64 \mu\text{b}$ [42] at mid-rapidity and $d\sigma_{J/\psi}/dy = 3.93 \mu\text{b}$ [40] at forward rapidity, $2.5 < y < 4$. For excited states, we adopt the direct-production cross-section ratio in pp collisions for $\psi(2S)$ to J/ψ as $N_{\psi(2S)}^{\text{PP}}/N_{J/\psi}^{\text{PP}} = 0.147$ [40] and $N_{\chi_c}^{\text{PP}}/N_{J/\psi}^{\text{PP}} = 0.926$ for χ_c [43].

For the initial charmonium phase-space distribution, $f(\mathbf{x}, \mathbf{P}_{\Psi}, t_0)$, we assume a factorization into three components: the spatial distribution, evaluated from a collision profile based on a Glauber model [44], the momentum spectrum, based on experimental data in pp collisions [40, 45–47], and the p_{T} -dependent shadowing estimated from ALICE J/ψ data [48] in pPb collisions (discussed below). We fit the inclusive J/ψ p_{T}

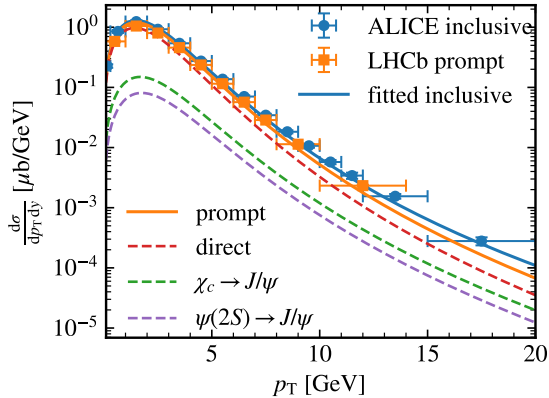


Fig. 7: Inclusive (blue solid line) and prompt (orange solid line) J/ψ transverse-momentum spectra in pp collisions at $\sqrt{s} = 5.02$ TeV. The prompt component is further decomposed into the direct contribution (red dashed line) and feeddown from χ_c (green dashed line) and $\psi(2S)$ (purple dashed line). The data are taken from ALICE [40] and LHCb [41].

spectrum measured at forward rapidity ($2.5 < y < 4$) in 5.02 TeV pp collisions [40] with a power-law ansatz

$$\frac{dN^{\text{pp}}}{dp_T} = \frac{N}{[1 + (p_T/A)^c]^n}, \quad (30)$$

with parameters $N=0.0599$, $A=3.81$, $c=2$, and $n=3.73$; at mid-rapidity, the corresponding fit to ALICE data [42] yields $N=0.043$, $A=4.48$, $c=2$, and $n=3.73$. The inclusive J/ψ yield can be decomposed into direct production, prompt feeddown from excited states (χ_c and $\psi(2S)$), and non-prompt feeddown from bottom-hadron decays. The non-prompt feeddown fraction is constrained by LHCb measurements at $\sqrt{s} = 5.02$ TeV [45], while the prompt feeddown fractions are taken from LHCb data at $\sqrt{s} = 7$ TeV [46, 47]. Figure 7 shows the resulting inclusive and prompt J/ψ p_T spectra in pp collisions at $\sqrt{s}=5.02$ TeV and forward rapidity, together with their decomposition into direct and feeddown contributions. For the inclusive $\psi(2S)$ spectrum at forward rapidity in pp collisions [40], the power-law fit yields $N=0.033$, $A=5.10$, $c=2$, and $n=3.70$. The non-prompt feeddown contribution to inclusive $\psi(2S)$ production is constrained using LHCb measurements at $\sqrt{s} = 7$ TeV [41].

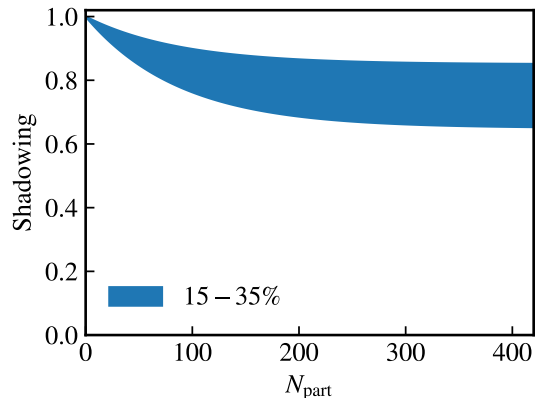
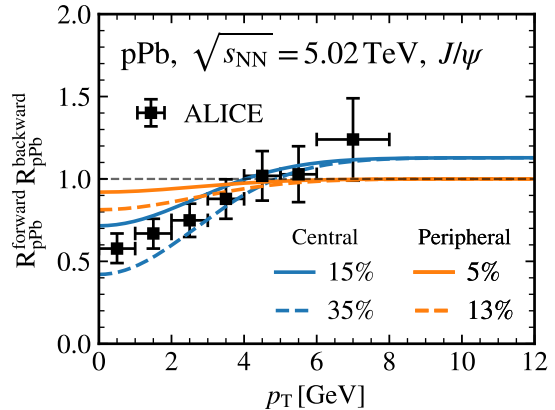


Fig. 8: Parameterizations of the nuclear-shadowing suppression of the $c\bar{c}$ production cross section. The upper panel shows the p_T dependence in p -Pb collisions, compared to ALICE data [48], while the lower panel shows the centrality dependence as a function of N_{part} in Pb-Pb collisions.

The $c\bar{c}$ production cross section in pp collisions is a key input for the charmonium equilibrium limit and thus controls the regeneration yield. For a given rapidity interval, the number of produced $c\bar{c}$ pairs is given by $dN_{c\bar{c}}/dy = (d\sigma_{c\bar{c}}/dy) N_{\text{coll}}/\sigma_{\text{pp}}^{\text{inel}}$, where $\sigma_{\text{pp}}^{\text{inel}}$ is the inelastic cross section in pp collisions. At mid-rapidity, the measured charm cross section amounts to $d\sigma_{c\bar{c}}/dy = 1.165 \pm 0.133$ mb [49]. We extrapolate this to forward rapidity using the rapidity dependence of Ref. [50], yielding $d\sigma_{c\bar{c}}/dy = 0.72 \pm 0.07$ mb, where a 10% uncertainty is assigned. The initial spatial distribution of c -quarks is sampled from the Glauber model [44], while

the transverse momenta (p_T) are from Fixed-Order Next-to-Leading-Logarithm (FONLL) calculations [51], which we fit with the same ansatz as in Eq. (30) resulting in the parameter values $N=0.045$, $A=3.3$, $c=2.2$, and $n=2.7$. The longitudinal momentum distribution is assumed to be thermal.

Finally, we account for cold-nuclear-matter (CNM) effects which modify both the magnitude and p_T dependence of the charm(onium) production cross sections in the Pb–Pb environment. The impact on the c -quark p_T spectrum is implemented through a multiplicative modification factor adopted from Ref. [52],

$$S_c(p_T) = a_1 e^{-b_1(p_T-d_1)} + c_1 + a_2 e^{-b_2(p_T-d_2)}, \quad (31)$$

where the parameters are given as

$$\begin{aligned} a_1 &= -0.27, & b_1 &= 0.17, & d_1 &= 1.00, \\ a_2 &= -65.39, & b_2 &= 0.52, & d_2 &= -11.14, \\ c_1 &= 1.02. \end{aligned}$$

The CNM effect for charmonium p_T spectra is estimated using ALICE data [48] on J/ψ production in p -Pb collisions at forward and backward rapidities, $2.5 < |y| < 4$. We fit the product of the measured forward and backward nuclear modification factors, R_{pPb} , which can be interpreted as the net effect of shadowing in Pb–Pb collisions, as shown in the upper panel of Fig. 8. For central collisions, we estimate a suppression of 15–35% of the integrated yield stemming from shadowing, with a p_T dependence that reproduces the forward-backward R_{pPb} product. For peripheral collisions, the shadowing effect is significantly reduced: with a 15–35% suppression in central collisions, the suppression in peripheral collisions amounts to about 5–13%, extrapolated from central collisions using a centrality dependence parameterized through an effective nuclear absorption cross section within the Glauber model [53]. In contrast to central collisions, no anti-shadowing behavior is assumed at large p_T for peripheral collisions. The N_{part} dependence of the shadowing for the $c\bar{c}$ production cross section is also assumed to reach values of 15–35%, in line with our previous study [10], as displayed in the lower panel of Fig. 8.

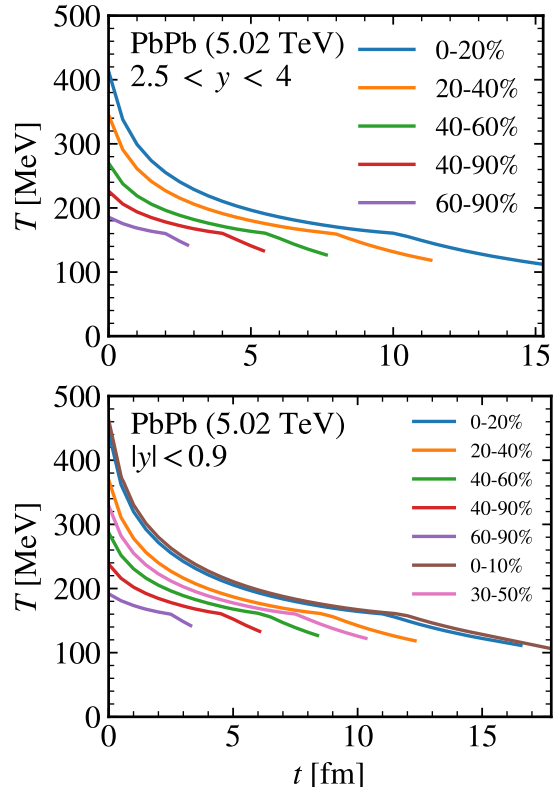


Fig. 9: Time evolution of the temperature of the expanding-fireball model at different centralities at forward (upper panel) and mid-rapidity (lower panel). At a “hadronization” temperature of $T_H = 170$ MeV, the equation of state is switched from lattice QCD to a hadron resonance gas model (not visible in the plots). The kink in each curve occurs at the hadro-chemical freeze-out temperature of $T_{ch} = 160$ MeV, below which effective hadronic chemical potentials ensure the conservation of the observed light-hadron yields.

4.2 Time evolution of Ψ yields

To enable a better understanding of how the charm-charmonium kinetics manifests itself under the conditions of heavy-ion reactions, and ultimately in the final charmonium yields, we first discuss the time dependence of their various components in the hot fireballs with the inputs specified in the previous section. For now, we employ a schematic (isotropic and isentropic) fireball model where the total entropy is fixed by the finally observed light-hadron abundances at a given centrality while the expansion is simulated

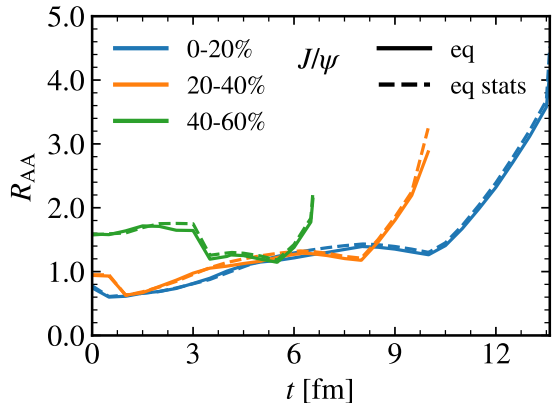


Fig. 10: Equilibrium limit of J/ψ as a function of time for different collision centralities (colors). Dashed lines correspond to the equilibrium limit from the statistical model, while solid lines show the result from our transport approach in the charm-quark thermalization limit.

by a time-dependent blast-wave description whose parameters are chosen to mimic hydrodynamic evolutions with endpoints (*i.e.*, thermal freezeout) that are in the range of extractions from experimental p_T spectra, cf. also Ref. [10]. The resulting temperature evolution is shown in Fig. 9 at mid- and forward rapidities and for different centrality classes. Clearly, future studies will have to improve on this framework.

In a first step, we display in Fig. 10 the R_{AA} for the J/ψ equilibrium limit (without any feeddown) obtained from our coupled transport approach assuming fully thermalized charm quarks, and compare that to the results from the statistical model, as a function of time at different centralities (a similar check has also been reported in Ref. [54]). The two results are in good agreement and consistent with the analytical derivation presented above. The R_{AA} values are rather large, close to one or even higher, and two structures are discernible: a drop-off at relatively early times (except for central collisions), which is an effect of the correlation volume, and a late-time increase which is due to the switch in degrees of freedom from partonic to hadronic at $T_H = 170$ MeV.

With the equilibrium benchmark in place, we show in Fig. 11 the time evolution of the primordial, regenerated and equilibrium limits

of charmonium R_{AA} 's in central and peripheral Pb–Pb ($\sqrt{s_{NN}} = 5.02$ TeV) collisions at forward rapidity. Here, the equilibrium limit is obtained from the detailed balance relation, Eq. (17), with time-dependent off-equilibrium charm-quark momentum distributions as follows from the Langevin simulations. Compared to the statistical-equilibrium limit, it is substantially reduced, with the effect being more pronounced in peripheral collisions where the shorter fireball lifetime and lower temperatures limit c -quark thermalization, compared to central collisions. This reduction is understood to be a consequence of harder c -quark distributions which have less favorable phase space for bound-state formation [23] (it was implemented in our previous works through a thermal-relaxation time approximation [22]). In our current setup we do not account for open-charm diffusion in the hadronic phase; we therefore utilize the reduction of the equilibrium limit from the QGP phase at $T_H = 170$ MeV to continuously match it to the hadronic phase and use the same rescaling factor throughout the hadronic medium evolution. The regeneration rate in the hadronic phase is then computed from the rescaled equilibrium limit and the hadronic reaction rate through the detailed-balance relation [9].

In central collisions, both primordial J/ψ and $\psi(2S)$ states experience strong suppression due to the large reaction rates in the strongly coupled QGP, and their primordial yields are essentially eliminated at early times. As a result, the final yields are dominated by regeneration. The regenerated J/ψ gradually approaches its equilibrium limit during the QGP evolution. After about ~ 6 fm/c, when the temperature has dropped below ~ 190 MeV and the reaction rate is below 100 MeV, the regeneration yield of the J/ψ levels off. On the other hand, the $\psi(2S)$, due to its larger rates, reaches its equilibrium limit within ~ 1 – 2 fm/c after regeneration sets in and stays rather close to it also at later stages. In peripheral collisions, the timescales are much shorter, which implies much reduced regeneration while a significant portion of the primordially produced states survives.

4.3 Centrality dependence

We are now in position to extract the R_{AA} observables from our coupled charm-charmonium transport framework, starting with the centrality

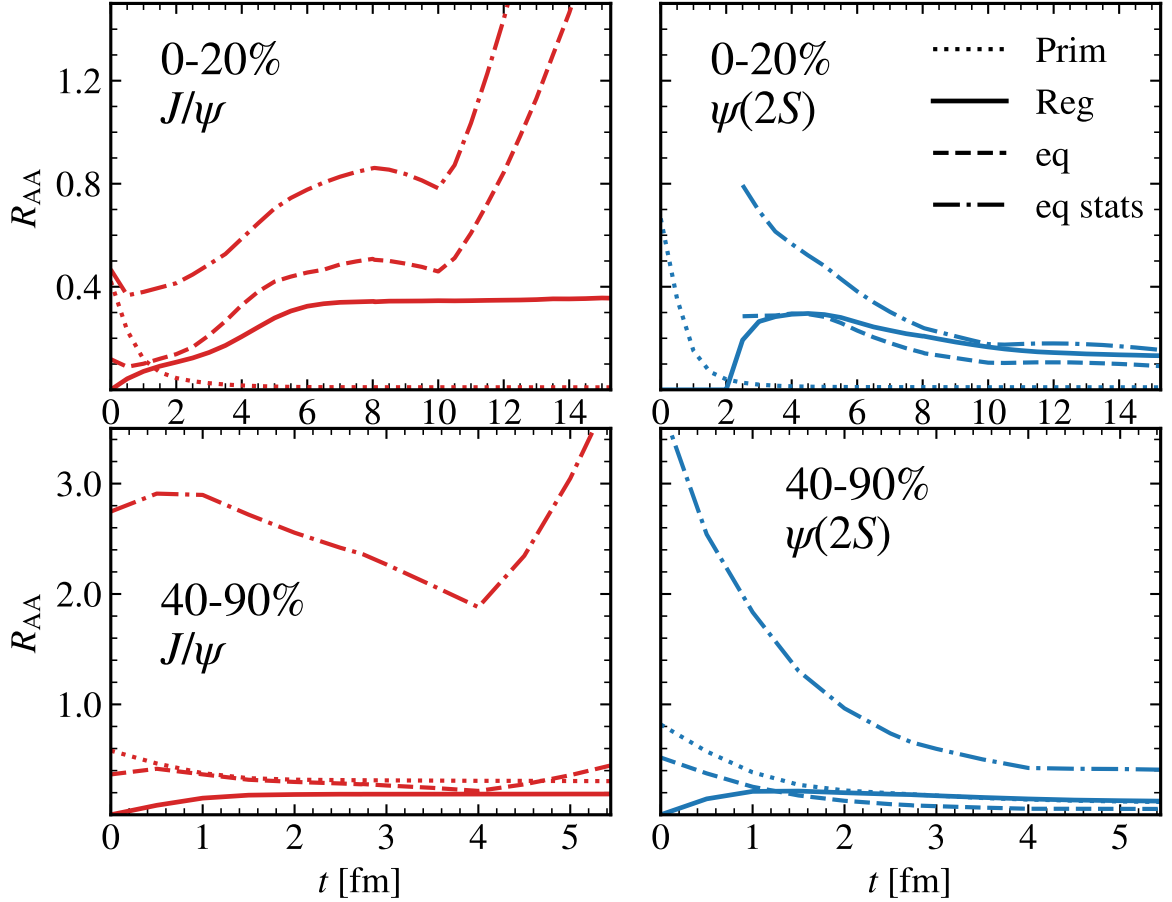


Fig. 11: Time evolution of charmonium R_{AA} of 1S (left) and 2S (right) in central (top) and peripheral (bottom) Pb–Pb collisions at $\sqrt{s_{NN}} = 5.02$ TeV at forward rapidity. The dash-dotted line denotes the equilibrium limit from the statistical model, the dashed line the equilibrium limit including off-equilibrium effects. Solid and dotted lines represent regenerated and primordial components, respectively.

dependence of charmonium production at forward/backward and mid-rapidity, summarized in the upper and lower panels of Fig. 12, respectively. For the J/ψ , the strong dissociation rate at high temperatures leads to a pronounced suppression in semi-central and central collisions, while the increasing charm-quark multiplicity toward central events enhances the regeneration contribution. As a result, the total R_{AA} develops a broad minimum around $N_{\text{part}} \simeq 100 - 150$ followed by a rise toward most central collisions. This trend is more pronounced at mid-rapidity and is consistent with the picture that primordial charmonia are largely depleted in the hottest QGP regions,

whereas subsequent recombination partially compensates for the loss. There is a slight tendency to underestimate the data at mid to peripheral centrality, where multiple pairs of charm quarks are produced but not in sufficient numbers to reach the grand canonical limit. More rigorous treatments of the canonical ensemble and the correlation volume are needed here. Additionally, a realistic hydrodynamic medium evolution could improve the description of flow effects for mid to peripheral centrality.

For $\psi(2S)$, the suppression is significantly stronger due to its weaker binding and ensuing larger rates. The regeneration contribution is smaller compared to J/ψ , mostly reflecting both

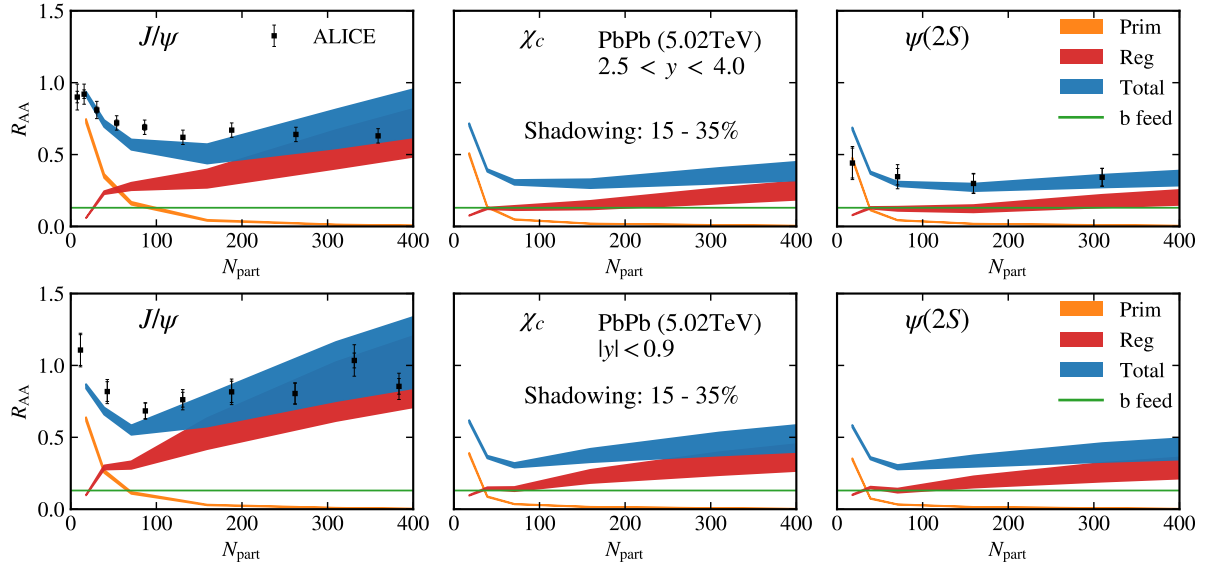


Fig. 12: Centrality dependence of the nuclear modification factors for J/ψ (left panels) χ_c (middle panels) and $\psi(2S)$ (right panels) production in Pb–Pb (5.02 TeV) collisions at forward/backward (top row) and mid-rapidity (bottom row). The bands for the primordial (orange), regenerated (red), and total (blue) components include uncertainties from nuclear shadowing on both open and hidden charm initial production. The calculations for J/ψ and $\psi(2S)$ are compared to ALICE data [55–57].

the reduced statistical weight. Consequently, after a steep initial suppression in peripheral collisions, the total R_{AA} exhibits a much weaker rise with centrality. The model reproduces the overall magnitude and slope of the ALICE measurements at forward rapidity fairly well.

The χ_c results follow a pattern very similar to that of $\psi(2S)$: a strong primordial suppression and a rather moderate regeneration component with a slightly stronger increasing trend compared to the $\psi(2S)$ but still significantly less than the J/ψ . Since χ_c feeddown constitutes a sizable fraction of the inclusive J/ψ yield in pp collisions, its suppression also plays a role in shaping the observed J/ψ spectra.

4.4 Transverse-momentum spectra

The interplay of (suppressed) primordial production and regeneration is expected to leave distinct signatures in the charmonium p_T -spectra [59]. In Figs. 13+14 and Fig. 15 we summarize our results for the $R_{AA}(p_T)$'s of J/ψ , $\psi(2S)$, and χ_c states at forward rapidity and mid-rapidity, respectively.

For the J/ψ the low- p_T enhancement due to regeneration, followed by a transition to a primordial component, reproduces the data fairly well. There is some underestimation of the ALICE data in the transition regime for mid-central collisions, a feature that we also found in our previous calculations with a perturbative medium coupling. This may be remedied by the inclusion of space-momentum correlations (SMCs) between the diffusing quarks and the expanding medium which are not accounted for in our present treatment, but which largely resolved this problem in a hydrodynamic treatment in Ref. [60]. On the other hand, the overestimate of the low- p_T data in peripheral collisions is much less severe than in our previous calculations [10] owing to the use of off-equilibrium c -quark spectra, as opposed to the blast-wave approximation in our previous work. The R_{AA} 's of the excited states share largely similar features, although the low- p_T enhancement is less pronounced since the regeneration is limited by the significantly smaller equilibrium limits at the R_{AA} level. The only data available for those are the $\psi(2S)$ in minimum-bias collisions, cf. the left panel in Fig. 14.

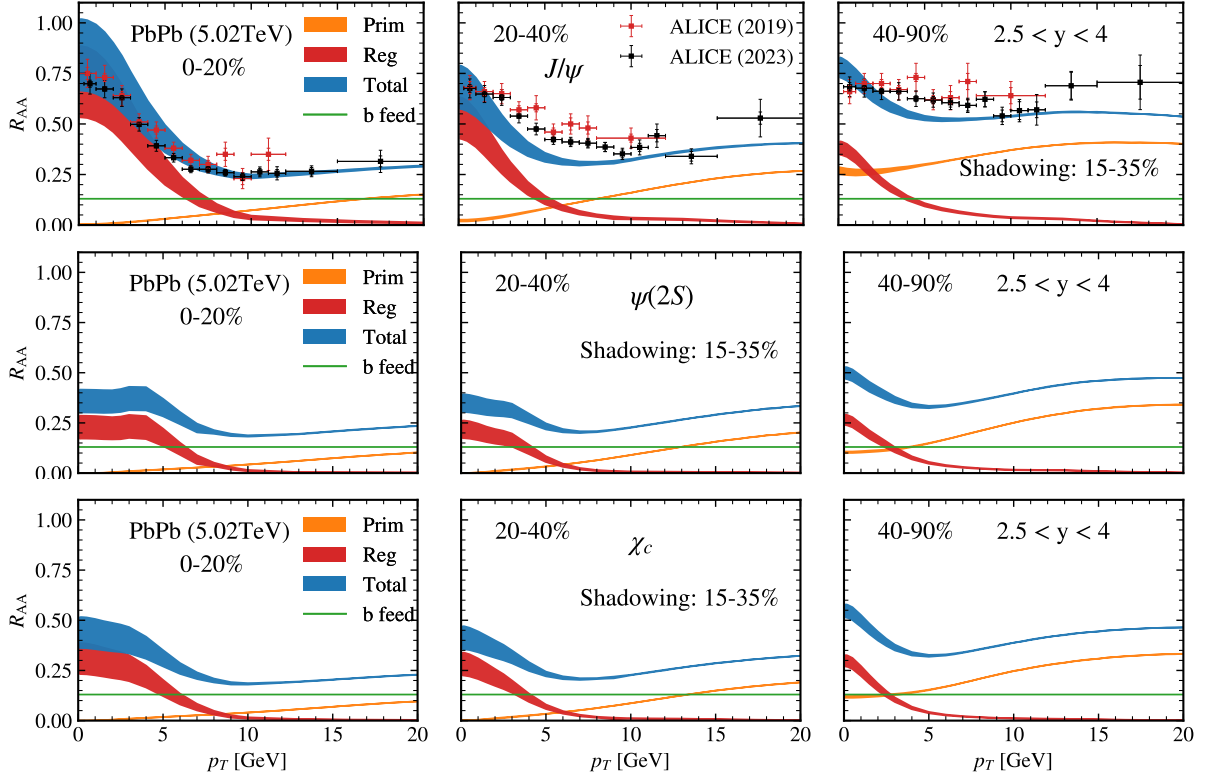


Fig. 13: Transverse-momentum–dependent nuclear modification factor, R_{AA} , of inclusive J/ψ , (top row), $\psi(2S)$ (middle row) and χ_c (bottom row) production in Pb–Pb ($\sqrt{s_{NN}}=5.02$ TeV) collisions at forward rapidity. The bands represent the primordial (orange), regenerated (red), and total (blue) contributions, including uncertainties from nuclear shadowing. The contribution from B -hadron feeddown (green) is taken as a constant fraction of 13%. The calculations are compared to ALICE data [57, 58].

For all three states, the suppression of primordial production at high p_T is less pronounced than that at low p_T . This is due to the reduced rates at high p_T as well as Lorentz time dilation on the formation time effects during the expansion of the charmonium wave packet. The escape effect, *i.e.* primordial charmonia leaving the medium, also leads to less suppression at high p_T , although this effect is less important than the former two.

The results at mid-rapidity, displayed in Fig. 15, largely mirror the findings at forward y , although with some increase in the R_{AA} values at low p_T due to the stronger regeneration at larger charm cross section and stronger suppression reflecting the longer fireball lifetime and higher initial temperatures. For the 30-50% centrality class, the same problem as for the mid-central forward- y calculations is apparent, namely

that the J/ψ R_{AA} underestimates the data in the intermediate- p_T region around 5 GeV. Again, a more realistic hydrodynamic medium and, in particular, SMCs are likely to improve on this.

5 Conclusions

In the present work we have developed a coupled transport approach where the diffusion of heavy quarks is directly coupled to the kinetics of quarkonia in a strongly coupled QGP. Recent calculations of charm and charmonium transport coefficients based on the same underlying microscopic interactions have been implemented into a coupled set of Langevin-Boltzmann equations. While the latter correspond to a semiclassical approximation, the transport coefficients follow from nonperturbative T -matrix interactions

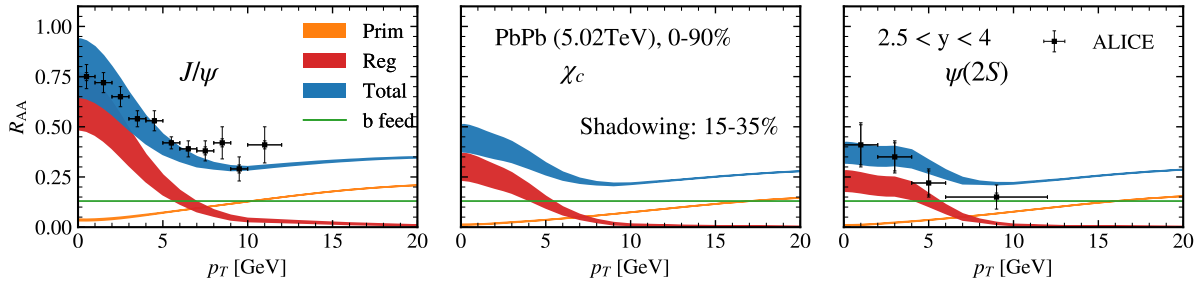


Fig. 14: Same as Fig. 13 but for minimum-bias (0-90%) Pb-Pb ($\sqrt{s_{\text{NN}}}=5.02$ TeV) collisions for J/ψ (left panel), χ_c (middle panel) and $\psi(2S)$ (right panel) mesons. The calculations of J/ψ and $\psi(2S)$ are compared to ALICE data [55, 56].

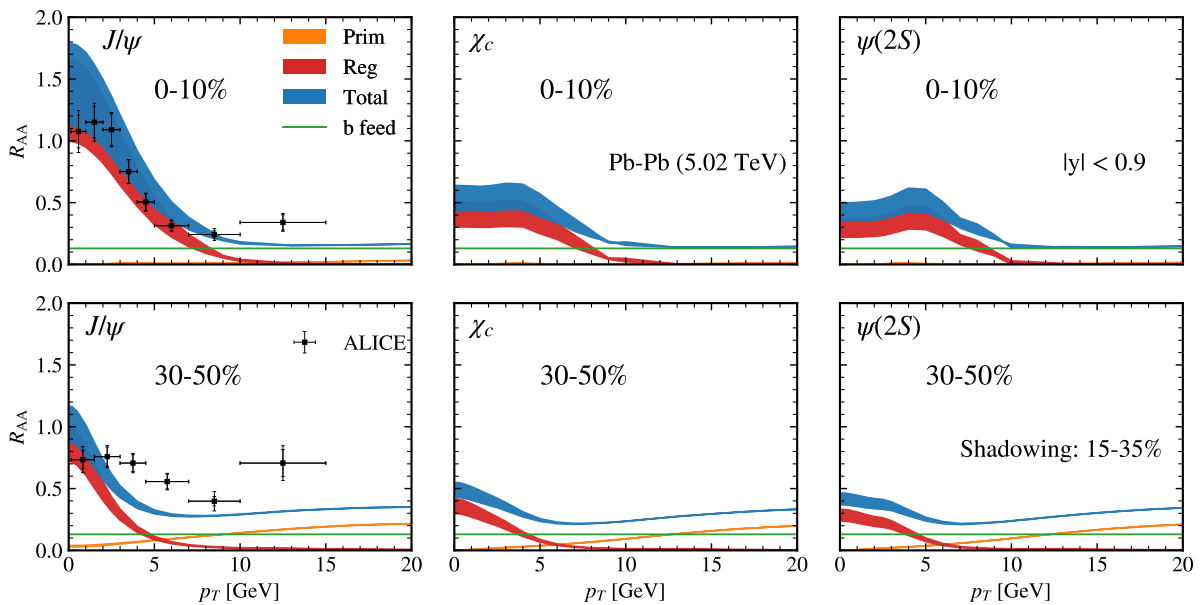


Fig. 15: Transverse-momentum dependent R_{AA} at mid-rapidity for inclusive J/ψ (first column), χ_c (second column), and $\psi(2S)$ (third column) production in Pb-Pb ($\sqrt{s_{\text{NN}}}=5.02$ TeV) collisions, for 0-10% (top row) and 30-50% (bottom row) centrality selections. Line identifications as in Fig. 13. The J/ψ calculations are compared to ALICE measurements [57].

whose in-medium driving kernel (*i.e.*, HQ potential) is constrained by state-of-the-art Wilson-line correlators computed in thermal lattice-QCD. This, in particular, accounts for quantum effects in the sQGP driven by the large collision rates of the charm quarks and thermal-medium partons which are encoded in the transport coefficients by pertinent off-shell spectral functions. The charm-quark transport coefficients have recently been deployed

in open HF phenomenology at the LHC and found to be compatible with D -meson observables without the use of any K -factors. An essential feature of our semiclassical simulations is that they recover the correct (thermal and chemical) equilibrium limit for charmonia for the case of thermalized charm quarks for an arbitrary number of pairs in the system, which is critical given

the large reaction rates in the sQGP. The charmonium equilibrium limits have been constrained by lattice-QCD data for open-charm susceptibilities, and an off-shell extension of the regeneration rate with in-medium spectral functions has been constructed that maintains detailed balance with earlier calculated dissociation rates. In this way, the impact of the gradual thermalization in the open-charm sector on charmonium kinetics can be controlled, thus replacing earlier employed relaxation-time approximations. The general feature of a suppression of regeneration due to incomplete c -quark thermalization persists, even at a semi-quantitative level.

We have conducted a preliminary application to charmonium data from Pb–Pb collisions at the LHC using a schematic fireball model. Compared to our previous work, the much larger rates substantially accelerate the suppression of the primordial component, especially at low p_T , essentially wiping it out in (semi-) central collisions up to about $p_T \simeq 5(2)$ GeV. At the same time, the regenerated yields reach close to the “equilibrium” limit but with incomplete c -quark thermalization. The latter is particularly relevant also in peripheral collisions, where the resulting, much flatter p_T spectra remedied an overshoot at low p_T that was found when using a blast-wave approximation. Overall, the agreement with the J/ψ data is fair, especially given that there was no fine-tuning of the transport parameters, *i.e.*, the charmonium reaction rates and equilibrium limits, as well as the c -quark diffusion. Our results tend to have a somewhat stronger increase of the yields with centrality than the data suggest and a deficit at intermediate p_T for semi-central collisions. The use of a more realistic viscous hydrodynamic medium evolution and the inclusion of space-momentum correlations are candidates to improve on that.

Several future developments, especially in the phenomenological implementation, are in order. A first step is to embed the transport dynamics into hydrodynamic simulations of the space-time evolution of the bulk medium, and to incorporate the aforementioned space-momentum correlations between the medium and (fast-moving) charm quarks. While quantum transport for multiple pairs remains very challenging, the current use of formation time effects in the evolution of the individual primordial wave packets warrants a

more rigorous (quantum) treatment. Furthermore, simulations of the coupled dynamics of $c\bar{c}$ pairs as microscopic degrees of freedom, rather than treating charm quarks and charmonia as independent particles, should be further investigated, see, *e.g.*, Refs. [61–63], possibly to serve as mutual benchmarks.

Acknowledgments

We thank X. Du for helpful discussions. This work is supported by the U.S. National Science Foundation under grant nos. PHY-2209335 and 2514775 and by the Department of Energy via the Topical Collaboration in Nuclear Theory on *Heavy-Flavor Theory (HEFTY) for QCD Matter* under award no. DE-SC0023547.

References

- [1] Matsui, T., Satz, H.: J/ψ Suppression by Quark-Gluon Plasma Formation. *Phys. Lett. B* **178**, 416–422 (1986)
- [2] Rapp, R., Blaschke, D., Crochet, P.: Charmonium and bottomonium production in heavy-ion collisions. *Prog. Part. Nucl. Phys.* **65**, 209–266 (2010) <https://doi.org/10.1016/j.ppnp.2010.07.002> [arXiv:0807.2470](https://arxiv.org/abs/0807.2470) [hep-ph]
- [3] Braun-Munzinger, P., Stachel, J.: Charmonium from Statistical Hadronization of Heavy Quarks – a Probe for Deconfinement in the Quark-Gluon Plasma. *Landolt-Bornstein* **23**, 424 (2010) https://doi.org/10.1007/978-3-642-01539-7_14 [arXiv:0901.2500](https://arxiv.org/abs/0901.2500) [nucl-th]
- [4] Mocsy, A., Petreczky, P., Strickland, M.: Quarkonia in the Quark Gluon Plasma. *Int. J. Mod. Phys. A* **28**, 1340012 (2013) <https://doi.org/10.1142/S0217751X13400125> [arXiv:1302.2180](https://arxiv.org/abs/1302.2180) [hep-ph]
- [5] Andronic, A., *et al.*: Comparative study of quarkonium transport in hot QCD matter. *Eur. Phys. J. A* **60**(4), 88 (2024) <https://doi.org/10.1140/epja/s10050-024-01306-6> [arXiv:2402.04366](https://arxiv.org/abs/2402.04366) [nucl-th]
- [6] Braun-Munzinger, P., Stachel, J.:

- (Non)thermal aspects of charmonium production and a new look at J/ψ suppression. *Phys. Lett. B* **490**, 196–202 (2000) [https://doi.org/10.1016/S0370-2693\(00\)00991-6](https://doi.org/10.1016/S0370-2693(00)00991-6) [arXiv:nucl-th/0007059](https://arxiv.org/abs/hep-th/0007059)
- [7] Thews, R.L., Schroedter, M., Rafelski, J.: Enhanced J/ψ production in deconfined quark matter. *Phys. Rev. C* **63**, 054905 (2001) <https://doi.org/10.1103/PhysRevC.63.054905> [arXiv:hep-ph/0007323](https://arxiv.org/abs/hep-ph/0007323)
- [8] Grandchamp, L., Rapp, R.: Thermal versus direct J/ψ production in ultrarelativistic heavy ion collisions. *Phys. Lett. B* **523**, 60–66 (2001) [https://doi.org/10.1016/S0370-2693\(01\)01311-9](https://doi.org/10.1016/S0370-2693(01)01311-9) [arXiv:hep-ph/0103124](https://arxiv.org/abs/hep-ph/0103124)
- [9] Du, X., Rapp, R.: Sequential Regeneration of Charmonia in Heavy-Ion Collisions. *Nucl. Phys. A* **943**, 147–158 (2015) <https://doi.org/10.1016/j.nuclphysa.2015.09.006>
- [10] Wu, B., Rapp, R.: Charmonium Transport in Heavy-Ion Collisions at the LHC. *Universe* **10**(6), 244 (2024) <https://doi.org/10.3390/universe10060244> [arXiv:2404.09881](https://arxiv.org/abs/2404.09881) [nucl-th]
- [11] Shuryak, E.V.: What RHIC experiments and theory tell us about properties of quark-gluon plasma? *Nucl. Phys. A* **750**, 64–83 (2005) <https://doi.org/10.1016/j.nuclphysa.2004.10.022> [arXiv:hep-ph/0405066](https://arxiv.org/abs/hep-ph/0405066)
- [12] Hees, H., Greco, V., Rapp, R.: Heavy-quark probes of the quark-gluon plasma at RHIC. *Phys. Rev. C* **73**, 034913 (2006) <https://doi.org/10.1103/PhysRevC.73.034913> [arXiv:nucl-th/0508055](https://arxiv.org/abs/nucl-th/0508055) [nucl-th]
- [13] Beraudo, A., *et al.*: Extraction of Heavy-Flavor Transport Coefficients in QCD Matter. *Nucl. Phys. A* **979**, 21–86 (2018) <https://doi.org/10.1016/j.nuclphysa.2018.09.002> [arXiv:1803.03824](https://arxiv.org/abs/1803.03824) [nucl-th]
- [14] Altenkort, L., Cruz, D., Kaczmarek, O., Larsen, R., Moore, G.D., Mukherjee, S., Petreczky, P., Shu, H.-T., Stendebach, S.: Quark Mass Dependence of Heavy Quark Diffusion Coefficient from Lattice QCD. *Phys. Rev. Lett.* **132**(5), 051902 (2024) <https://doi.org/10.1103/PhysRevLett.132.051902> [arXiv:2311.01525](https://arxiv.org/abs/2311.01525) [hep-lat]
- [15] Tang, Z., Mukherjee, S., Petreczky, P., Rapp, R.: T-matrix analysis of static Wilson line correlators from lattice QCD at finite temperature. *Eur. Phys. J. A* **60**(4), 92 (2024) <https://doi.org/10.1140/epja/s10050-024-01310-w> [arXiv:2310.18864](https://arxiv.org/abs/2310.18864) [hep-lat]
- [16] Wu, B., Rapp, R.: Bottomonium transport in a strongly coupled quark-gluon plasma. *Phys. Lett. B* **873**, 140223 (2026) <https://doi.org/10.1016/j.physletb.2026.140223> [arXiv:2508.20995](https://arxiv.org/abs/2508.20995) [nucl-th]
- [17] Bala, D., Kaczmarek, O., Larsen, R., Mukherjee, S., Parkar, G., Petreczky, P., Rothkopf, A., Weber, J.H.: Static quark-antiquark interactions at nonzero temperature from lattice QCD. *Phys. Rev. D* **105**(5), 054513 (2022) <https://doi.org/10.1103/PhysRevD.105.054513> [arXiv:2110.11659](https://arxiv.org/abs/2110.11659) [hep-lat]
- [18] Krishna, T., Rapp, R., Fu, Y., Bass, S.A., Ke, W.: Nonperturbative heavy-flavor transport approach for hot QCD matter. *Phys. Lett. B* **871**, 139999 (2025) <https://doi.org/10.1016/j.physletb.2025.139999> [arXiv:2509.13881](https://arxiv.org/abs/2509.13881) [nucl-th]
- [19] Wu, B., Tang, Z., Rapp, R.: Non-perturbative quarkonium dissociation rates in strongly coupled quark-gluon plasma. *JHEP* **07**, 162 (2025) [https://doi.org/10.1007/JHEP07\(2025\)162](https://doi.org/10.1007/JHEP07(2025)162) [arXiv:2503.10089](https://arxiv.org/abs/2503.10089) [nucl-th]
- [20] Thapa, S., Wu, B., Vogt, R., Rapp, R.: Semiclassical treatment of bottomonium suppression and regeneration in $p + \text{Pb}$ collisions (2025) [arXiv:2510.03456](https://arxiv.org/abs/2510.03456) [nucl-th]
- [21] Tang, Z., Wu, B., Hanlon, A., Mukherjee, S., Petreczky, P., Rapp, R.: Quarkonium Spectroscopy in the Quark-Gluon Plasma. *Phys. Rev. Lett.* **135**(14), 142302 (2025) <https://doi.org/10.1103/7zby-gy46> [arXiv:2502.09044](https://arxiv.org/abs/2502.09044) [nucl-th]

- [22] Grandchamp, L., Rapp, R.: Charmonium suppression and regeneration from SPS to RHIC. Nucl. Phys. A **709**, 415–439 (2002) [https://doi.org/10.1016/S0375-9474\(02\)01027-8](https://doi.org/10.1016/S0375-9474(02)01027-8) arXiv:hep-ph/0205305
- [23] Song, T., Han, K.C., Ko, C.M.: Charmonium production from nonequilibrium charm and anticharm quarks in quark-gluon plasma. Phys. Rev. C **85**, 054905 (2012) <https://doi.org/10.1103/PhysRevC.85.054905> arXiv:1203.2964 [nucl-th]
- [24] Moore, G.D., Teaney, D.: How much do heavy quarks thermalize in a heavy ion collision? Phys. Rev. C **71**, 064904 (2005) <https://doi.org/10.1103/PhysRevC.71.064904> arXiv:hep-ph/0412346
- [25] Hees, H., Rapp, R.: Thermalization of heavy quarks in the quark-gluon plasma. Phys. Rev. C **71**, 034907 (2005) <https://doi.org/10.1103/PhysRevC.71.034907> arXiv:nucl-th/0412015
- [26] Mustafa, M.G.: Energy loss of charm quarks in the quark-gluon plasma: Collisional versus radiative. Phys. Rev. C **72**, 014905 (2005) <https://doi.org/10.1103/PhysRevC.72.014905> arXiv:hep-ph/0412402
- [27] Du, X., Rapp, R.: Non-equilibrium charmonium regeneration in strongly coupled quark-gluon plasma. Phys. Lett. B **834**, 137414 (2022) <https://doi.org/10.1016/j.physletb.2022.137414> arXiv:2207.00065 [nucl-th]
- [28] Svetitsky, B.: Diffusion of charmed quarks in the quark-gluon plasma. Phys. Rev. D **37**, 2484–2491 (1988)
- [29] Rapp, R., Hees, H.: In: Hwa, R., Wang, X.N. (eds.) Quark-Gluon Plasma 4, p. 111. World Scientific, Singapore (2010)
- [30] He, M., Hees, H., Gossiaux, P.B., Fries, R.J., Rapp, R.: Relativistic Langevin Dynamics in Expanding Media. Phys. Rev. E **88**, 032138 (2013) <https://doi.org/10.1103/PhysRevE.88.032138> arXiv:1305.1425 [nucl-th]
- [31] Liu, S.Y.F., He, M., Rapp, R.: Probing the in-Medium QCD Force by Open Heavy-Flavor Observables. Phys. Rev. C **99**(5), 055201 (2019) <https://doi.org/10.1103/PhysRevC.99.055201> arXiv:1806.05669 [nucl-th]
- [32] Yan, L., Zhuang, P., Xu, N.: j/ψ production in quark-gluon plasma. Phys. Rev. Lett. **97**, 232301 (2006) <https://doi.org/10.1103/PhysRevLett.97.232301>
- [33] Grandchamp, L., Rapp, R., Brown, G.E.: In medium effects on charmonium production in heavy ion collisions. Phys. Rev. Lett. **92**, 212301 (2004) <https://doi.org/10.1103/PhysRevLett.92.212301> arXiv:hep-ph/0306077
- [34] Laine, M., Philipsen, O., Romatschke, P., Tassler, M.: Real-time static potential in hot QCD. JHEP **0703**, 054 (2007)
- [35] Zhao, X., Rapp, R.: Charmonium in Medium: From Correlators to Experiment. Phys. Rev. C **82**, 064905 (2010) <https://doi.org/10.1103/PhysRevC.82.064905> arXiv:1008.5328 [hep-ph]
- [36] Du, X., He, M., Rapp, R.: Color Screening and Regeneration of Bottomonia in High-Energy Heavy-Ion Collisions. Phys. Rev. C **96**(5), 054901 (2017) <https://doi.org/10.1103/PhysRevC.96.054901> arXiv:1706.08670 [hep-ph]
- [37] Hamieh, S., Redlich, K., Tounsi, A.: Canonical description of strangeness enhancement from p-A to Pb Pb collisions. Phys. Lett. B **486**, 61–66 (2000) [https://doi.org/10.1016/S0370-2693\(00\)00762-0](https://doi.org/10.1016/S0370-2693(00)00762-0) arXiv:hep-ph/0006024
- [38] Bellwied, R., Borsanyi, S., Fodor, Z., Katz, S.D., Pasztor, A., Ratti, C., Szabo, K.K.: Fluctuations and correlations in high temperature QCD. Phys. Rev. D **92**(11), 114505 (2015) <https://doi.org/10.1103/PhysRevD.92.114505> arXiv:1507.04627 [hep-lat]
- [39] Kaczmarek, O., Karsch, F., Petreczky,

- P., Schmidt, C., Sharma, S.: Generalized susceptibilities and the properties of charm degrees of freedom across the QCD crossover temperature. *Phys. Rev. D* **112**(3), 034509 (2025) <https://doi.org/10.1103/tz74-d3kh> [arXiv:2505.01734](https://arxiv.org/abs/2505.01734) [hep-lat]
- [40] Acharya, S., *et al.*: Inclusive quarkonium production in pp collisions at $\sqrt{s} = 5.02$ TeV. *Eur. Phys. J. C* **83**(1), 61 (2023) <https://doi.org/10.1140/epjc/s10052-022-10896-8> [arXiv:2109.15240](https://arxiv.org/abs/2109.15240) [nucl-ex]
- [41] Aaij, R., *et al.*: Measurement of $\psi(2S)$ production cross-sections in proton-proton collisions at $\sqrt{s} = 7$ and 13 TeV. *Eur. Phys. J. C* **80**(3), 185 (2020) <https://doi.org/10.1140/epjc/s10052-020-7638-y> [arXiv:1908.03099](https://arxiv.org/abs/1908.03099) [hep-ex]
- [42] Acharya, S., *et al.*: Inclusive J/ψ production at mid-rapidity in pp collisions at $\sqrt{s} = 5.02$ TeV. *JHEP* **10**, 084 (2019) [https://doi.org/10.1007/JHEP10\(2019\)084](https://doi.org/10.1007/JHEP10(2019)084) [arXiv:1905.07211](https://arxiv.org/abs/1905.07211) [nucl-ex]
- [43] Navas, S., *et al.*: Review of particle physics. *Phys. Rev. D* **110**(3), 030001 (2024) <https://doi.org/10.1103/PhysRevD.110.030001>
- [44] Miller, M.L., Reygers, K., Sanders, S.J., Steinberg, P.: Glauber modeling in high energy nuclear collisions. *Ann. Rev. Nucl. Part. Sci.* **57**, 205–243 (2007) <https://doi.org/10.1146/annurev.nucl.57.090506.123020> [arXiv:nucl-ex/0701025](https://arxiv.org/abs/nucl-ex/0701025)
- [45] Aaij, R., *et al.*: Measurement of J/ψ production cross-sections in pp collisions at $\sqrt{s} = 5$ TeV. *JHEP* **11**, 181 (2021) [https://doi.org/10.1007/JHEP11\(2021\)181](https://doi.org/10.1007/JHEP11(2021)181) [arXiv:2109.00220](https://arxiv.org/abs/2109.00220) [hep-ex]
- [46] Aaij, R., *et al.*: Measurement of the ratio of prompt χ_c to J/ψ production in pp collisions at $\sqrt{s} = 7$ TeV. *Phys. Lett. B* **718**, 431–440 (2012) <https://doi.org/10.1016/j.physletb.2012.10.068> [arXiv:1204.1462](https://arxiv.org/abs/1204.1462) [hep-ex]
- [47] Aaij, R., *et al.*: Measurement of $\psi(2S)$ meson production in pp collisions at $\sqrt{s}=7$ TeV. *Eur. Phys. J. C* **72**, 2100 (2012) <https://doi.org/10.1140/epjc/s10052-012-2100-4> [arXiv:1204.1258](https://arxiv.org/abs/1204.1258) [hep-ex]. [Erratum: *Eur.Phys.J.C* 80, 49 (2020)]
- [48] Adam, J., *et al.*: Rapidity and transverse-momentum dependence of the inclusive J/ψ nuclear modification factor in p-Pb collisions at $\sqrt{s_{NN}} = 5.02$ TeV. *JHEP* **06**, 055 (2015) [https://doi.org/10.1007/JHEP06\(2015\)055](https://doi.org/10.1007/JHEP06(2015)055) [arXiv:1503.07179](https://arxiv.org/abs/1503.07179) [nucl-ex]
- [49] Acharya, S., *et al.*: Charm-quark fragmentation fractions and production cross section at midrapidity in pp collisions at the LHC. *Phys. Rev. D* **105**(1), 011103 (2022) <https://doi.org/10.1103/PhysRevD.105.L011103> [arXiv:2105.06335](https://arxiv.org/abs/2105.06335) [nucl-ex]
- [50] Bierlich, C., Wilkinson, J., Sun, J., Manca, G., Cassagnac, R., Otwinowski, J.: Open charm production cross section from combined LHC experiments in pp collisions at $\sqrt{s} = 5.02$ TeV. *Eur. Phys. J. Plus* **139**(7), 593 (2024) <https://doi.org/10.1140/epjp/s13360-024-05355-0> [arXiv:2311.11426](https://arxiv.org/abs/2311.11426) [hep-ph]
- [51] Cacciari, M., Frixione, S., Houdeau, N., Mangano, M.L., Nason, P., Ridolfi, G.: Theoretical predictions for charm and bottom production at the LHC. *JHEP* **10**, 137 (2012) [https://doi.org/10.1007/JHEP10\(2012\)137](https://doi.org/10.1007/JHEP10(2012)137) [arXiv:1205.6344](https://arxiv.org/abs/1205.6344) [hep-ph]
- [52] Emel'yanov, V., Khodinov, A., Klein, S.R., Vogt, R.: Charm quark production in non-central heavy ion collisions. *Phys. Rev. C* **56**, 2726–2735 (1997) <https://doi.org/10.1103/PhysRevC.56.2726> [arXiv:nucl-th/9706085](https://arxiv.org/abs/nucl-th/9706085)
- [53] Zhao, X., Rapp, R.: Forward and midrapidity charmonium production at RHIC. *Eur. Phys. J. C* **62**, 109–117 (2009) <https://doi.org/10.1140/epjc/s10052-009-0905-6> [arXiv:0810.4566](https://arxiv.org/abs/0810.4566) [nucl-th]
- [54] Zhao, S., He, M.: Simulation of heavy quarkonium equilibration in the quark-gluon plasma. *Phys. Rev. D* **112**(9), 094018 (2025) <https://doi.org/10.1103/4rdc-9dkx>

- arXiv:2508.11897 [hep-ph]
- [55] Adam, J., *et al.*: J/ψ suppression at forward rapidity in Pb-Pb collisions at $\sqrt{s_{NN}} = 5.02$ TeV. Phys. Lett. B **766**, 212–224 (2017) <https://doi.org/10.1016/j.physletb.2016.12.064> arXiv:1606.08197 [nucl-ex]
- [56] Acharya, S., *et al.*: $\psi(2S)$ Suppression in Pb-Pb Collisions at the LHC. Phys. Rev. Lett. **132**(4), 042301 (2024) <https://doi.org/10.1103/PhysRevLett.132.042301> arXiv:2210.08893 [nucl-ex]
- [57] Acharya, S., *et al.*: Measurements of inclusive J/ψ production at midrapidity and forward rapidity in Pb-Pb collisions at $s_{NN} = 5.02$ TeV. Phys. Lett. B **849**, 138451 (2024) <https://doi.org/10.1016/j.physletb.2024.138451> arXiv:2303.13361 [nucl-ex]
- [58] Acharya, S., *et al.*: Studies of J/ψ production at forward rapidity in Pb-Pb collisions at $\sqrt{s_{NN}} = 5.02$ TeV. JHEP **02**, 041 (2020) [https://doi.org/10.1007/JHEP02\(2020\)041](https://doi.org/10.1007/JHEP02(2020)041) arXiv:1909.03158 [nucl-ex]
- [59] Zhao, X., Rapp, R.: Transverse Momentum Spectra of J/ψ in Heavy-Ion Collisions. Phys. Lett. B **664**, 253–257 (2008) <https://doi.org/10.1016/j.physletb.2008.03.068> arXiv:0712.2407 [hep-ph]
- [60] He, M., Wu, B., Rapp, R.: Collectivity of J/ψ Mesons in Heavy-Ion Collisions. Phys. Rev. Lett. **128**(16), 162301 (2022) <https://doi.org/10.1103/PhysRevLett.128.162301> arXiv:2111.13528 [nucl-th]
- [61] Young, C., Shuryak, E.: Charmonium in strongly coupled quark-gluon plasma. Phys. Rev. C **79**, 034907 (2009) <https://doi.org/10.1103/PhysRevC.79.034907> arXiv:0803.2866 [nucl-th]
- [62] Oei, N., Krenz, N., Hees, H., Greiner, C., Torres-Rincon, J.M.: Formation, dissociation, and regeneration of charmonia within microscopic Langevin simulations. Phys. Rev. D **111**(7), 074012 (2025) <https://doi.org/10.1103/PhysRevD.111.074012> arXiv:2410.19619 [hep-ph]
- [63] Daddi-Hammou, A., Delorme, S., Blaizot, J.-P., Gossiaux, P.B., Gousset, T.: Quantum vs semiclassical description of in-QGP quarkonia in the quantum Brownian regime. Phys. Rev. D **113**(1), 014017 (2026) <https://doi.org/10.1103/kyc5-mrj3> arXiv:2506.19194 [hep-ph]